Chinese Chemical Letters 32 (2021) 48–52

Contents lists available at ScienceDirect

Chinese Chemical Letters

journal homepage: www.elsevier.com/locate/cclet

Communication

Low-temperature and stable CO oxidation of Co_3O_4/TiO_2 monolithic catalysts

Xinyue Tang[a,b], Junchao Wang[a], Yonghui Ma[d], Jing Li[c], Xinglai Zhang[a], Baodan Liu[c,*]

[a] Shenyang National Laboratory for Materials Science, Institute of Metal Research, Chinese Academy of Sciences, Shenyang 110016, China
[b] School of Materials Science and Engineering, University of Science and Technology of China, Shenyang 110016, China
[c] Foshan Graduate School of Northeastern University, Foshan 528300, China
[d] Structure Analysis Division, Testing Center, Institute of Metal Research, Chinese Academy of Science, Shenyang 110016, China

ARTICLE INFO

Article history:
Received 15 July 2020
Received in revised form 16 September 2020
Accepted 3 November 2020
Available online 4 November 2020

Keywords:
Co_3O_4/TiO_2
In-situ growth
Monolithic catalysts
Long-term stability
CO oxidation

ABSTRACT

Highly efficient Co_3O_4/TiO_2 monolithic catalysts with enhanced stability were *in-situ* grown on Ti mesh for CO oxidation, which could completely oxidize CO at 120 °C. The comprehensive catalytic performance is competitive to some noble metal catalysts and conventional Co_3O_4 powder catalysts, which holds great potential toward industrial applications. Meanwhile, the *in-situ* synthesis strategy of Co_3O_4/TiO_2 monolithic catalysts on flexible mesh substrate in this work can be extended to the development of a variety of oxide-based monolithic catalysts towards diverse catalysis applications.

Toxic CO exhaust emission in industrial processes and vehicle combustions is harmful to mammals and vegetation and contributes to global warming [1,2]. The conversion of CO gas into non-toxic CO_2 has been regarded as the most efficient and economical ways to remove CO among all the CO elimination methods. In this way, noble-metal catalysts, such as Au, Pd, Rh, have been demonstrated to exhibit high catalytic activity towards CO oxidation [3–5]. However, the low abundance, high costs, and unsatisfactorily thermal stability of these noble metal catalysts hinder the industrial application and drive us to search for alternative substitution catalysts for efficient and low temperature CO oxidation. Among the readily available low-cost catalysts, Co_3O_4 is considered as a promising non-noble metal catalyst to replace noble metals owing to its high activity for low temperature CO oxidation [6–8]. It has been reported that the morphology of Co_3O_4 plays a vital role in catalysis performance and can be designed through given preparation methods such as sol-gel methods [9], template methods [10], solid-state chemical method [11], precipitation methods [12], hydrothermal method [13].

As demonstrated in numerous works, the fine tailoring and accurate control of nanostructure morphology can be easily realized by hydrothermal method [14–16]. Xie and Shen *et al.* [17] synthesized Co_3O_4 nanorods with exposed (110) plane primarily through hydrothermal method and a complete CO oxidation can be obtained at −77 °C. Liu *et al.* [18] also synthesized ultrathin two-dimensional (2D) Co_3O_4 nanoplates with exposed surfaces of (112) and the 100% CO conversion was achieved at ambient temperatures even under ultrahigh weight hourly space velocity (WHSV) about 750,000 mL g^{-1} h^{-1}. Although Co_3O_4 is extremely active for CO oxidation, the poor catalytic stability is still an important concern that limits its wide application. To obtain monolithic catalysts, the active powders are always fixed on ceramics or alloy supports using binders, which, consequently, takes the risk of peeling off during long term reaction due to the weak adhesion and discrepant thermal expansion between supports and active component. Hence, the development of Co_3O_4 monolithic catalysts with efficient activity and high stability is in need urgently.

In this work, we demonstrated the *in-situ* growth of Co_3O_4/TiO_2 monolithic catalysts on flexible Ti mesh substrate through scalable plasma electrolytic oxidation (PEO) technology associated with hydrothermal method (HR). Flexible Ti mesh as support can reduce the possibility of thermal inactivation due to the superior thermal conductivity. The *in-situ* growth of Co_3O_4 cocatalysts by HR ensures the tight combination with TiO_2 support. On these basis, Co_3O_4/TiO_2 monolithic catalysts with both high catalytic performance and

* Corresponding author.
E-mail address: baodanliu@hotmail.com (B. Liu).

https://doi.org/10.1016/j.cclet.2020.11.008

strong stability can be obtained. The microstructures, interfaces and CO oxidation performance of Co_3O_4/TiO_2 catalysts are also well studied using series of characterization techniques.

The specific preparation process of Co_3O_4/TiO_2 monolithic catalysts is elaborated in supplementary information and is schematically shown in Scheme S1 (Supporting information). The fast surface oxidation of Ti mesh *via* energetic PEO process enables superior mechanical contact between porous TiO_2 film and Ti substrate [19,20]. Meanwhile, the porous PEO film (anatase TiO_2), serving as the seed layer, is crucial to the *in-situ* preparation of TiO_2 nanosheet according to our previous studies [21,22]. The ultra-thin TiO_2 nanosheets can not only reduce the transfer path of inner electron to the surface that enables a fast catalytic reaction, [22] but also hold excellent oxygen storage capacity (OSC) [23,24], and the large specific surface area of TiO_2 nanosheet support can also provide sufficient active sites for the nucleation of Co_3O_4 cocatalyst with homogeneous distribution. The successful modification of highly active Co_3O_4 cocatalyst is confirmed by X-ray diffraction (XRD) results as shown in Fig. 1. The catalyst precursors of $Co(OH)_2$ (JCPDS No. 74-1057) and $H_2Ti_2O_5$ (JCPDS No. 47-1024) will be converted into final spinel Co_3O_4 (JCPDS No. 71-0816) and anatase TiO_2 (JCPDS No. 21-1272) phases after the annealing process. As shown in Fig. S1 (Supporting information), the morphology collapse and roughing occur due to the phase transformation from $Co(OH)_2$ to Co_3O_4. The ultra-thin Co_3O_4 nanoplate consists of numerous nanoparticles, which can provide sufficient active sites for CO oxidation. During HR process, the morphology of $Co(OH)_2$ precursor can be selectively controlled and well maintained after final calcination. The field-emission scanning electron microscopy (FESEM) images of final Co_3O_4/TiO_2 catalysts with different HR time are shown in Fig. 1. Evidently, TiO_2 nanosheets are uniformly covered with dense and aligned Co_3O_4 cocatalysts after the HR reaction and the calcination process. Co_3O_4 particles obtained by HR 1 h cannot be observed in SEM images due to their high dispersion or the ultrafine size, while the energy dispersive spectroscopy (EDS) results clearly indicate the existence of Co element (Fig. S2 in Supporting information). As the prolong of reaction time, the ultrathin Co_3O_4 nanoplate with irregular planar shape come into being and evolve to integrated nanoplates under 10 h reaction. With further increase of HR time, there is no significant change in morphology except for the obvious increase in thickness as shown in Fig. S3 (Supporting information). Meanwhile, the urea content also has significant influence on the Co_3O_4 morphology due to the different solution supersaturation (Fig. S4 in Supporting information). Similarly, only TiO_2 nanosheets can be observed at the low urea content. As the urea content increases from 8 mmol to 32 mmol, the thickness of Co_3O_4 nanoplates increases slightly. However, the excessive growth of Co_3O_4 nanoplate under 32 mmol urea will lead to obvious structural collapse and adhesion decrease due to the loose self-aggregation of tiny particles. The low magnification SEM image of monolithic mesh catalysts and the EDS mapping clearly indicate the homogeneous distribution of Co_3O_4 (Figs. S5 and S6 in Supporting information), and the weak signal of Ti element implies the dense covering of Co_3O_4 on TiO_2 nanosheets.

The morphological and structural features of Co_3O_4/TiO_2 catalysts are further investigated by transmission electron microscope (TEM) under high magnification. It is shown that the as synthesized Co_3O_4 nanoplates are composed of numerous nanoparticles with uniform size of about 40 nm (Figs. 2a–c and Fig. S7 in Supporting information). The lattice-resolved high-resolution TEM (HRTEM) analysis indicates that the Co_3O_4 nanoplate synthesized from multi-step process is highly crystallized and it exhibits a clear lattice fringe of 0.46 nm, corresponding to the (111) crystal plane of spinel Co_3O_4 phase (Fig. 2d). The fast Fourier transform (FFT) pattern (Fig. 2e) also matches well with the selected area electron diffraction (SAED) pattern of face-centered cubic Co_3O_4 taken along the $[01\bar{1}]$ zone axis. The elemental mappings of Co_3O_4/TiO_2 catalysts clearly show the homogeneous distribution of Co and O elements, while the weak signal of Ti indicates that TiO_2 nanosheets are covered by dense Co_3O_4 nanoplates (Figs. 2f–i). The good crystallinity, smaller size and uniform distribution of Co_3O_4 will undoubtedly favour the efficient low-temperature CO oxidation in practical application.

X-ray photoelectron spectroscopy (XPS) was used to analyse the oxidation states and the surface compositions of the Co_3O_4/TiO_2

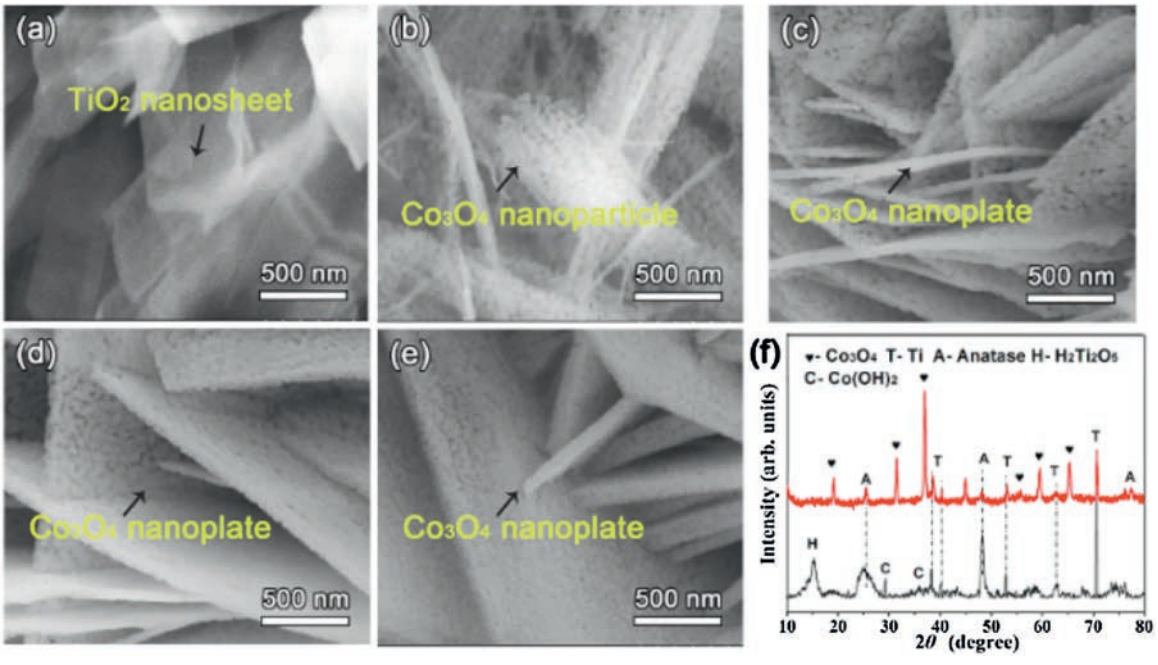

Fig. 1. SEM images of Co_3O_4/TiO_2 catalysts obtained by different HR time: (a) 1 h; (b) 5 h; (c) 10 h; (d) 15 h; (e) 20 h. (f) XRD pattern of precursor and final catalyst.

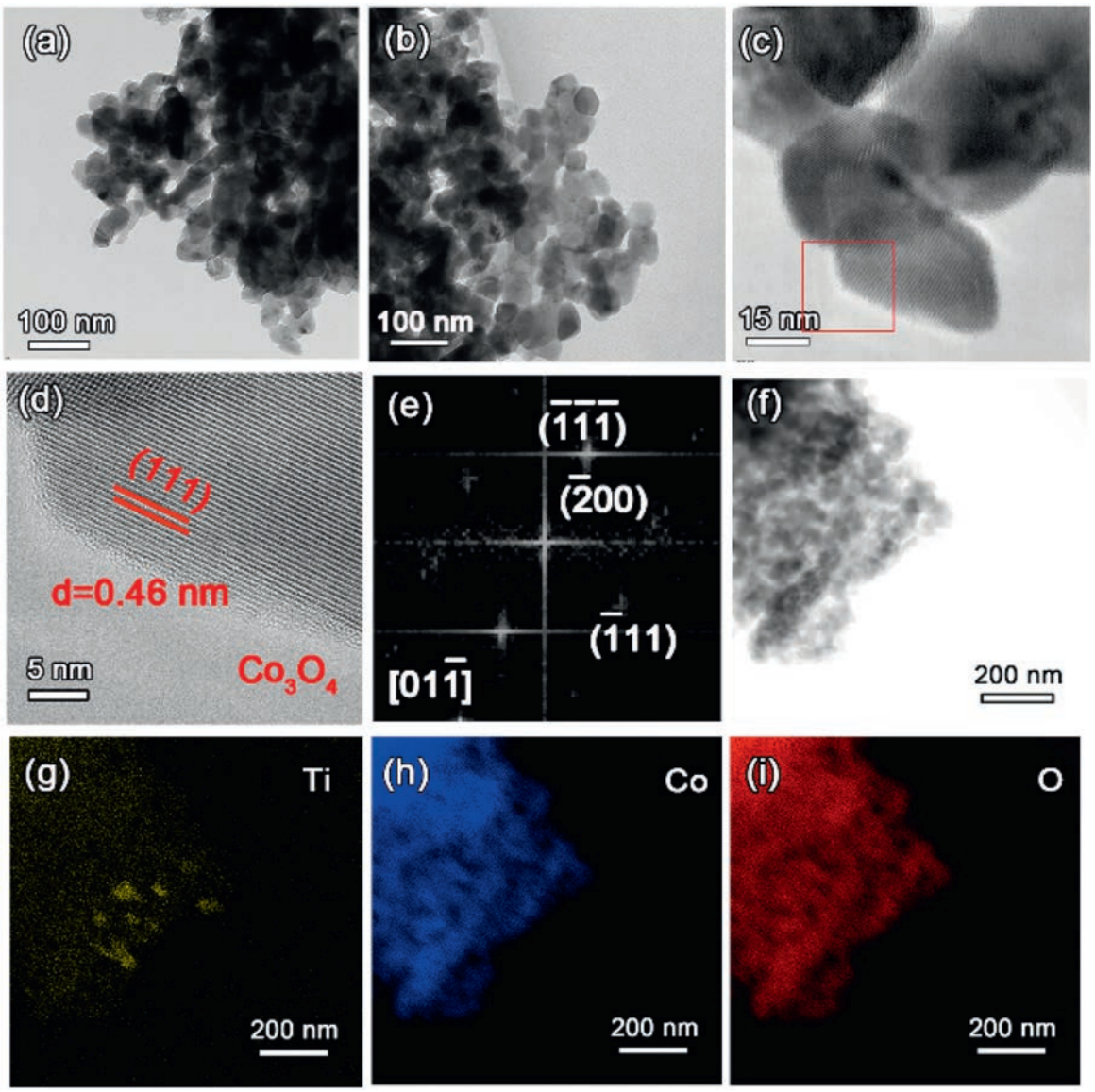

Fig. 2. (a,b) Representative low-magnification TEM image of Co_3O_4/TiO_2 catalyst. (c-e) HRTEM images and FFT patterns of Co_3O_4 nanoplate. (f) Bright-field TEM image of Co_3O_4/TiO_2 catalysts and (g-i) the elemental mapping of Co, Ti and O elements to show their spatial distribution.

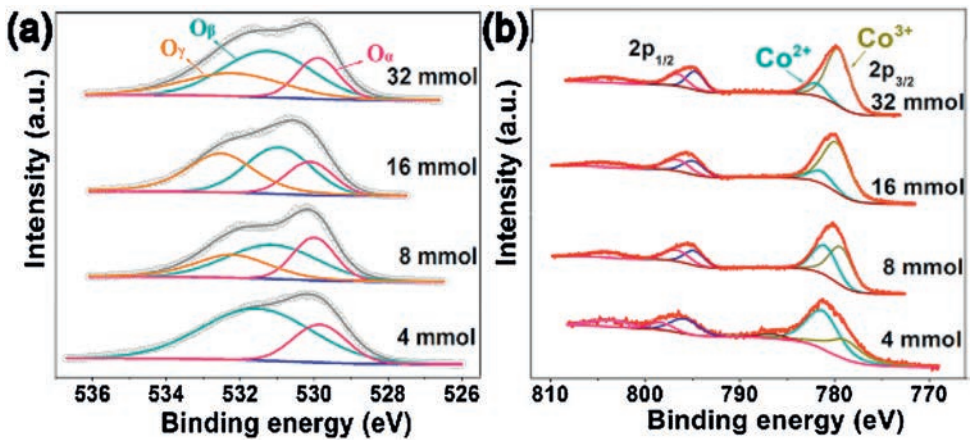

Fig. 3. XPS results of Co_3O_4/TiO_2 catalysts supported on Ti mesh synthesized by different urea concentration: (a) O 1s spectrum; (b) Co 2p spectrum.

catalysts synthesized under the urea content of 4–32 mmol (denoted as Co_3O_4 (4)-Co_3O_4 (32)). The characteristic peaks of Ti, O, Co and C can be clearly observed and two distinct peaks Ti 2p are the characteristic peaks of anatase TiO_2 as shown in Fig. S8 (Supporting information) [25]. Fig. 3a shows the O 1s spectra of the catalysts that can be divided into three components at ~529.5, 531.2 and 533.2 eV, which are assigned to lattice oxygen (O_α), adsorbed oxygen such as O^- or −OH (O_β), and oxygen in molecular water adsorbed on the catalyst surface (O_γ), respectively [26]. The ratios of different oxygen species over all the Co_3O_4/TiO_2 samples are listed in Table S1 (Supporting information). Obviously, the Co_3O_4 (32) sample presents a higher molar ratio of surface or chemisorbed oxygen (O_β + O_γ), implying the presence of more oxygen vacancies, which plays a prominent role in the catalytic performance CO oxidation [27]. With the increase of urea content, the oxygen vacancies also increase on the surface (Table S1). Therefore, it is speculated that the increase of oxygen vacancies may occur during the annealing process caused by the insufficient oxygen at interface of TiO_2/Co_3O_4 or the large thickness of Co_3O_4 nanoplates according to the SEM and XPS results and the improved catalytic performance of Co_3O_4 (32) discussed later also confirms the existence of more oxygen vacancies. Based on the electroneutrality principle, the increase of oxygen vacancies can be induced by the enhanced Co^{3+} species on the surface. As shown in Fig. 3b, the Co $2p_{3/2}$ peaks of the catalysts could be divided into Co^{3+} at about 779.2 ± 0.5 eV and Co^{2+} at about 781.2 ± 0.5 eV [28,29]. The proportion of Co^{3+} ion on the surface increases as urea concentration increases, while Co_3O_4 (4) shows a proportion of 29.4%. Among all these catalysts, the Co_3O_4 (32) catalyst shows the highest ratio of 80.0%, suggesting that the Co_3O_4/TiO_2 catalysts synthesized under high urea content have more highly active Co^{3+} ions. The rich Co^{3+} active sites on the surface of catalysts will result in enhanced activity doubtlessly [30].

As mentioned above, the different morphologies of Co_3O_4/TiO_2 catalysts are closely related to the surface area and the catalytic performance will be further affected. The BET surface area of Co_3O_4 (4)-Co_3O_4 (32) catalysts is measured and the results are listed in Table S2 (Supporting information). It can be seen that Co_3O_4 (32) has the largest surface area of 33.1 m^2/g, which is slightly higher than others. All the catalysts have the similar pore size distribution and average pore size, and produce Type IV adsorption isotherm with H3 type hysteresis in spite of the morphology difference, indicating the existence of mesopores (Fig. S9 and Table S2 in Supporting information) [31].

To evaluate the catalytic properties of the Co_3O_4/TiO_2 catalysts, CO oxidation as a probe reaction is carried out. Figs. 4a and b show the CO oxidation light-off curves of Co_3O_4/TiO_2 catalysts with different morphologies, and one can see that the complete conversion of CO to CO_2 can be achieved in the temperature range of 110–250 °C under normal feeding gas. It is found that the T_{100} (the temperature to 100% oxidize CO gas) gradually decreases as the increase of urea content and HR time, indicating that more Co_3O_4 cocatalysts favour the oxidation of CO gas (Fig. S10 in Supporting information). However, the excessive growth of Co_3O_4 nanoplates under 32 mmol urea or HR 20 h will lead to the peeling off due to the weak adhesion between Co_3O_4 and TiO_2 nanosheet support (Fig. S11 in Supporting information). To examine the contribution of Co_3O_4, the catalytic performance of TiO_2 nanosheets supported on Ti mesh without Co_3O_4 active component was investigated (Fig. S12 in Supporting information), and it was found that pure TiO_2 nanosheet can only completely oxidize CO gas molecular above 420 °C, which in turn indicates the excellent oxidation capability of Co_3O_4 nanostructures. In this regard, the Co_3O_4 (16) catalyst may have both high performance and superior adhesion for exceptional stability. As shown in Figs. 4c and d, the light-off curves of Co_3O_4 (16) catalysts after 2 months storage and

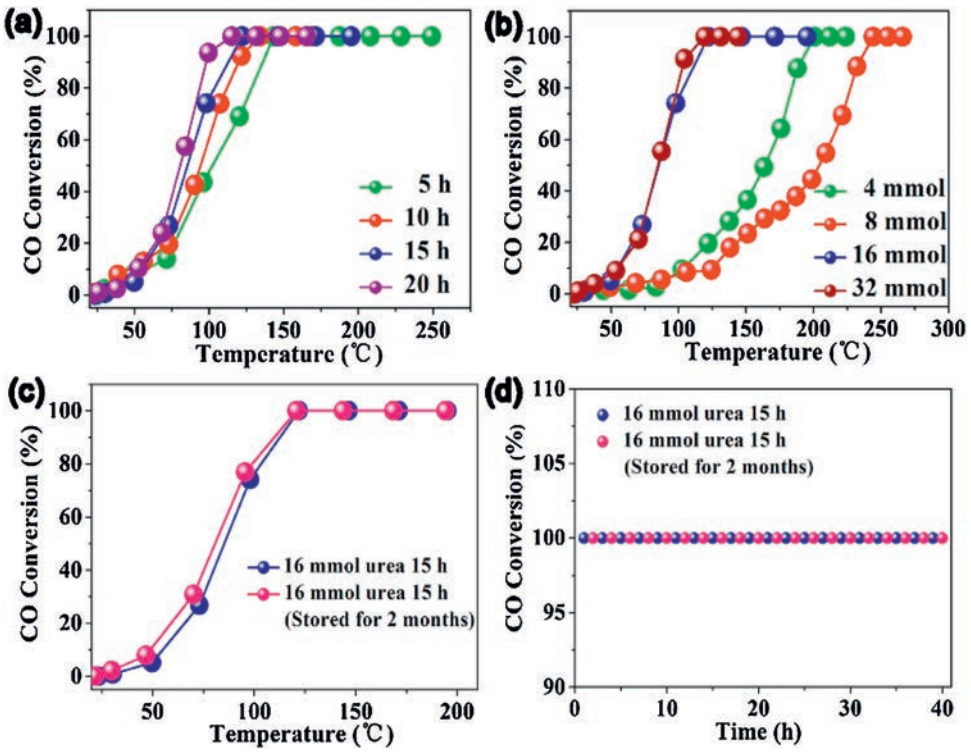

Fig. 4. Catalytic CO oxidation light-off curves of Co_3O_4/TiO_2 catalysts prepared with different (a) deposition time and (b) urea concentrations. (c) CO oxidation light-off curves of fresh catalysts and after two months. (d) Long-term catalytic stability tests at 120 °C for continuous 40 h.

the fresh one are almost the same, and the 100% CO conversion can be well maintained during continuous 40 h test at its T_{100} (120 °C). Even though the best T_{100} of Co_3O_4/TiO_2 catalysts is still higher than some pure Co_3O_4 nanorod catalysts, its oxidation capability is still more competitive and advantageous to some noble metal catalysts as listed in Table S3 (Supporting information). Especially, the sufficient reactive oxygen species, large specific area and short electron transfer path provided by TiO_2 nanosheets and the *in-situ* integration strategy of Co_3O_4/TiO_2 monolithic catalysts enable strong adhesion with beneath Ti mesh, which guarantees the superior long-term stability compared with other results reported literatures [11].

According to the XPS results and CO light-off curves, a possible scheme is proposed for the pathways of CO oxidation over the monolithic structured Co_3O_4/TiO_2 catalysts supported on Ti mesh. Previous studies have demonstrated that CO molecules are always adsorbed preferentially on Co^{3+} sites, which are generally considered as the active positions suitable for CO oxidation [32]. Meanwhile, abundant V_O on the catalyst surface will react with absorbed O_2 to form active oxygen species, which can react with adsorbed CO molecules and generate CO_2. The modification of Co_3O_4 cocatalyst through hydrothermal process produces rich oxygen vacancy on catalyst surface and ensures the high catalytic activity, which is competitive with some noble metals. Undoubtedly, the synthesized Co_3O_4/TiO_2 catalysts free of noble metal component will surely open up more opportunities for oxide-based catalysts towards long-term and efficient catalysis in diverse fields such as total oxidation (TOX), preferential catalytic oxidation of CO (PROX), three-way catalysis (TWCs) and selective catalytic reduction (SCR).

In conclusion, the synthesis of Co_3O_4/TiO_2 monolithic catalysts on flexible Ti mesh substrate was demonstrated through scalable PEO technology followed by hydrothermal treatment, and the high activity and superior stability in CO oxidation are confirmed. The *in-situ* nucleation of TiO_2 nanosheet substrate and Co_3O_4 cocatalyst provides strong adhesion to maintain the long-term stability, while the ultra-thin TiO_2 nanosheet offers sufficient active sites and fast electron transfer path to achieve outstanding CO oxidation capability. The full conversion of CO to CO_2 at temperature as low as 120 °C of Co_3O_4/TiO_2 monolithic catalysts is achieved, which is comparable or even superior to some noble metal catalysts. The *in-situ* integrated synthesis strategy holds great promise in industry and can open up more opportunities for the preparation of relevant monolithic catalysts for diverse applications.

Declaration of competing interest

The authors report no declarations of interest.

Acknowledgments

This work was partially supported by the National Natural Science Foundation of China (No. 51872296), the Joint Fund between Shenyang National Laboratory for Materials Science and State Key Laboratory of Advanced Processing and Recycling of Nonferrous Metals (No. 18LHPY012).

Appendix A. Supplementary data

Supplementary material related to this article can be found, in the online version, at doi:https://doi.org/10.1016/j.cclet.2020.11.008.

References

[1] E. Knözinger, A. Kellersohn, W. Langel, M. Giersig, Adv. Mater. 7 (1995) 652–655.
[2] M. Waqas, P.M. Kouotou, A.E. Kasmi, Y. Wang, Z. Tian, Chin. Chem. Lett. 31 (2019) 1201–1206.
[3] Y. Cai, Y. Guo, J. Liu, Chem. Commun. 56 (2020) 876–879.
[4] Y. Yan, H. Li, Z. Lu, et al., Chin. Chem. Lett. 30 (2019) 1153–1156.
[5] Z. Wu, D.R. Mullins, L.F. Allard, Q. Zhang, L. Wang, Chin. Chem. Lett. 29 (2018) 795–799.
[6] J. Bae, D. Shin, H. Jeong, et al., ACS Catal. 9 (2019) 10093–10100.
[7] Y. Lv, Y. Li, W. Shen, Catal. Commun. 42 (2013) 116–120.
[8] Y. Wang, Z. Chen, R. Fang, Y. Li, ChemCatChem 11 (2019) 772–779.
[9] F. Švegl, B. Orel, I. Grabec-Švegl, V. Kaučič, Electrochim. Acta 45 (2000) 4359–4371.
[10] D. Gu, C. Jia, C. Weidenthaler, et al., J. Am. Chem. Soc. 137 (2015) 11855–12160.
[11] K. Wang, Y. Cao, J. Hu, et al., ACS Appl. Mater. Inter. 9 (2017) 16128–16137.
[12] W. Tang, J. Weng, X. Lu, et al., Appl. Catal. B -Environ. 256 (2019) 117895.
[13] M. Li, F. Bi, Y. Xu, et al., ACS Catal. 9 (2019) 11676–11684.
[14] X. Xiao, X. Liu, H. Zhao, et al., Adv. Mater. 24 (2012) 5762–5766.
[15] K. Zhou, J. Liu, P. Wen, Y. Hu, Z. Gui, Mater. Res. Bull. 67 (2015) 87–93.
[16] Y. Liu, C. Mi, L. Su, X. Zhang, Electrochim. Acta 53 (2008) 2507–2513.
[17] X. Xie, Y. Li, Z.Q. Liu, M. Haruta, W. Shen, Nature 458 (2009) 746–749.
[18] Y. Cai, J. Xu, Y. Guo, J. Liu, ACS Catal. 9 (2019) 2558–2567.
[19] M. Shbeh, A. Yerokhin, R. Goodall, Appl. Surf. Sci. 439 (2018) 801–814.
[20] Y.K. Shin, W.S. Chae, Y.W. Song, Y.M. Sung, Electrochem. Commun. 8 (2006) 465–470.
[21] K. Wang, B. Liu, J. Li, et al., J. Mater. Sci. Technol. 35 (2019) 615–622.
[22] K. Wang, X. Liu, X. Tang, et al., Adv. Mater. Technol. (2020) 2000115.
[23] M. Kotobuki, R. Leppelt, D.A. Hansgen, D. Widmann, R.J. Behm, J. Catal. 264 (2009) 67–76.
[24] D. Widmann, E. Hocking, R.J. Behm, J. Catal. 317 (2014) 272–276.
[25] D. Guan, Y. Wang, Nanoscale 4 (2012) 2968–2977.
[26] Y. Liu, H. Dai, J. Deng, et al., Inorg. Chem. 52 (2013) 8665–8676.
[27] S. Mo, Q. Zhang, Y. Sun, et al., J. Mater. Chem. 7 (2019) 16197–16210.
[28] M. Zhou, L. Cai, M. Bajdich, et al., ACS Catal. 5 (2015) 4485–4491.
[29] Y. Lou, J. Ma, X. Cao, et al., ACS Catal. 4 (2014) 4143–4152.
[30] S. Mo, S. Li, J. Li, et al., Nanoscale 8 (2016) 15763–15773.
[31] H.M.A. Hassan, M.A. Betiha, R.F.M. Elshaarawy, M.S. El-Shall, Appl. Surf. Sci. 402 (2017) 99–107.
[32] B. Feng, M. Shi, J. Liu, et al., J. Hazard. Mater. 394 (2020) 122540–122553.